ELSEVIER

Chemical Engineering Journal 144 (2008) 245–258

Chemical Engineering Journal

www.elsevier.com/locate/cej

Sorption of Cu^{2+}, Cd^{2+}, and Pb^{2+} using modified zeolite from coal fly ash

Ronbanchob Apiratikul [a], Prasert Pavasant [a,b,*]

[a] *National Center of Excellence for Environmental and Hazardous Waste Management, Chulalongkorn University, Bangkok 10330, Thailand*
[b] *Department of Chemical Engineering, Faculty of Engineering, Chulalongkorn University, Bangkok 10330, Thailand*

Received 29 December 2006; received in revised form 14 January 2008; accepted 21 January 2008

Abstract

The coal fly ash (CFA) was modified to zeolite X using fusion method with cationic exchange capacity (CEC) of about 140 meq/100 g. The zeolite was used as an effective sorbent for Cu^{2+}, Cd^{2+}, and Pb^{2+}. The pseudo-second order kinetic model was appropriate for the description of the kinetic performance of the sorption. It required a longer time to reach equilibrium for higher initial metal concentration and lower sorbent dose but all reached equilibrium within 120 min. External mass transfer step seemed to take part as a rate limiting step for the sorption of Pb^{2+} at low initial concentration and high sorbent dose, on the contrary, the process was controlled more significantly by intraparticle diffusion step at high initial concentration and low sorbent dose. However, Cu^{2+} was found to be generally controlled by intraparticle diffusion step at all concentration range examined in this work. The sorption of Cd^{2+}, on the other hand was controlled both by external mass transfer and intraparticle diffusion steps at all range of initial concentration. Langmuir and Dubinin–Radushkevich isotherms were applied to describe equilibrium data. The order of maximum sorption capacity in a unit of mol kg^{-1} was: Pb^{2+} (2.03) > Cu^{2+} (1.43) > Cd^{2+} (0.870). The sorption energy fell in the range of physic-sorption. Equilibrium sorption capacity and removal percentage were governed by both initial concentration and sorbent dose. A general mathematical model was developed for describing the sorption under the variations in initial metal concentration and zeolite doses. This model was proven to be reasonably accurate with additional sets of experiments.

Keywords: Zeolite X; Heavy metals; Wastewater treatment; Kinetic; Isotherm

1. Introduction

The combustion of coal in the power plant generally creates a large quantity of fly ash (or coal fly ash, CFA) as a by-product. Several alternatives are proposed and implemented for the treatment of CFA, such as the use as cement supplement. This is because CFA possesses pozzolanic property [1]. In cases where there are no feasible economical options, they are mostly landfilled. CFA could also be used in the neutralization of acid mine drainage as reported by Somerset et al. [2]. Conversion CFA to zeolite is one of the potential alternatives for handling of the CFA as it is often constituted of high contents of silica and alumina which are the basic foundation in the formation of zeolite. Previous reports demonstrated the success in the conversion of CFA to zeolite. For instance, Faujasite and zeolite P were reported to be synthesized from the reaction between CFA and NaOH [3], whereas phillipsite and hibschite were found to occur from the reaction between lignite CFA and calcium hydroxide [4]. Zeolites are widely used in several applications such as catalysts for hydrogenation, alkylation, and isomerization, and sorbents for the removal of contaminants, e.g. heavy metals, toxic gas, dyes, and organic pollutants such as benzene and alcohol. Generally, there are two major methods in the synthesis of zeolite from CFA: hydrothermal and fusion methods, where the fusion method was reported to provide higher cation exchange capacity (CEC) than the hydrothermal at the same conditions, and therefore was considered more suitable for the adsorption of the cationic metal species [5].

For sorption applications, zeolites were often reported to exhibit high sorption capacity, sorption affinity, and cation exchange capacity for divalent sorbates. Lee et al. [6] reported that the synthesized zeolites from CFA had greater adsorption capabilities for Pb^{2+} than the original fly ash (6–7 times) and natural zeolites (3–5 times). Erdem et al. [7] reported that

* Corresponding author. Tel.: +662 218 6870; fax: +662 218 6877.
E-mail address: prasert.p@chula.ac.th (P. Pavasant).

1385-8947/$ – see front matter © 2008 Elsevier B.V. All rights reserved.
doi:10.1016/j.cej.2008.01.038

natural zeolites hold great potential for the sorption of several heavy metal cations, e.g. Co^{2+}, Cu^{2+}, Zn^{2+} and Mn^{2+}, and this could be used as alternative for activated carbon.

This work focused on the investigation of the conversion of CFA to zeolite, and the examination of the sorption characteristics and mechanism of the zeolite product in the removal of Cu^{2+}, Cd^{2+} and Pb^{2+} from aqueous solution was achieved through kinetic and equilibrium studies. A general mathematical model was proposed to describe the relationship between the initial concentration, sorbent dose and equilibrium sorption capacity/removal percentage of the metal.

2. Materials and methods

2.1. Preparation and characterization of sorbent

Coal fly ash was collected from the National Power Supply Co. Ltd., Prachinburi province, Thailand. The CFA was dried at 120 °C for 3 h before being stored in desiccators. This CFA was converted to zeolite using the fusion method as described in the work of Molina and Poole [5]. The method started with mixing CFA with ground NaOH anhydrous pellet at a weight ratio of about 1:1.75. The homogeneous mixture was then calcined in a nickel crucible at high temperature (550 °C) for 1 h. The fusion product was ground and transferred to a 250 mL Erlenmeyer flask with screw cap which contained 85 mL of deionized water, and then immerged in a shaker water bath at 30 °C for 24 h. The mixture was subsequently crystallized in an oven at 90 °C for 2 h. The solid product was separated from the solution using centrifugation and then washed with DI water until the pH of solution was down to 10–11 and then dried overnight (about 12 h) at 110 °C.

Cation exchange capacity of the zeolite product was determined using Sodium acetate method according to the US-EPA method 9081 [8]. The product was then analyzed with X-Ray Diffractometer, SIEMENS (D5000), to investigate the zeolitic phase using Cu Kα radiation (λ = 0.154056 nm), with Ni filter. The X-Ray Fluoresence spectrophotometer, ARL, 9400 was used to determine the overall mineral composition of the product. The dry solid samples were analyzed for density in gas (helium) and water pycnometers. The particle size distribution (PSD) of product was determined by Laser Particle Size Analyzer, Malvern, Mastersizer-S long bed Version 2.19 using water as a medium. The Surface area analyzer, Thermo Finnigan, Sorptomatic 1990 was used for determining the specific surface area (SAA), whereas the total pore volume (TPV) of the product was determined using BET technique based on adsorption characteristics of N_2 gas on the sample at 77 K. The point of zero charge (PZC) was determined by measuring the surface charge of product in the DI water solution at various pH using Zeta Meter electrophoresis, Zeiss/3.0+. The pH of DI water was adjusted by nitric acid and sodium hydroxide to the desired pH.

2.2. Experimental procedure of sorption study

To determine the effect of initial concentration on sorption kinetics, the experiment was performed by mixing 0.03 g dried zeolite in 30 mL of the synthetic metal ion solution (sorbent dose = 1.0 g L^{-1}) with an initial metal concentration in the range of 0–5 mol m^{-3}. The pH was chemically controlled at five using CH_3COONH_4/CH_3COOH buffer system. The mixtures were mixed in a rotary shaker at a rate of 150 rpm for 0–2 h and the temperature of the solution was controlled at 21 ± 2 °C. Suspended solids were separated out with GF/C filter. Metal ions concentrations were then measured in the filtrate by atomic absorption spectrophotometer (AAS). Experiments were repeated at least three times to ensure the accuracy of the results. More repetitions were carried out in cases where %relative standard deviation exceeded 15%.

To investigate the sorbent dose on sorption kinetics, the experiment was conducted in a similar fashion with that described in the previous paragraph. However, in this experiment, the initial concentration was fixed at 5 mol m^{-3} whereas the sorbent dose was varied in the range of 0.5–3 g L^{-1}.

The equilibrium sorption experiments were conducted using the sorbent dose in the range of 0.5–3 g L^{-1} and the initial concentration in the range of 0–8 mol m^{-3} at the contact time of 120 min, the same conditions as those stated in the first paragraph of this section.

2.3. Calculations

2.3.1. Removal efficiency and sorption capacity of metal ions

The removal efficiency of metal ion is calculated from:

$$\%\text{Removal} = \frac{(C_o - C_f)}{C_o} \times 100 \quad (1)$$

The sorption capacity of metal ion is the amount of metal ion sorbed on the zeolite which can be calculated based on the mass balance principle where:

$$q = \frac{V(C_o - C_f)}{m} \quad (2)$$

In these two equations, q represents the amount of metal uptaken per unit mass of the zeolite (mol kg^{-1}), V the volume of the solution (m^3), m the dry mass of the zeolite (kg), C_o and C_f initial and final concentrations (mol m^{-3}), respectively.

2.3.2. Sorption kinetic model based on reaction order

Two sorption kinetic models were used in this work to describe the sorption characteristics. The first model was the pseudo-first order rate equation developed by Lagergren [9]. The model can be expressed in Eq. (3)

$$\frac{dq}{dt} = k_1(q_e - q) \quad (3)$$

Integrating Eq. (3) from $t = 0$ to $t = t$ and $q = 0$ to $q = q$ results in:

$$q = q_e(1 - e^{-k_1 t}) \quad (4)$$

The second model was pseudo-second order rate equation as expressed in Eq. (5) [10–14].

$$\frac{dq}{dt} = k_2(q_e - q)^2 \quad (5)$$

Integrating Eq. (5) from $t=0$ to $t=t$ and $q=0$ to $q=q$ leads to:

$$q = \frac{q_e^2 k_2 t}{1 + q_e k_2 t} \tag{6}$$

In Eqs. (3)–(6), t is the contact time (min), q the sorption capacity of metal ion at time (mol kg^{-1}), q_e the sorption capacity at equilibrium (mol kg^{-1}), k_1 the first order rate constant (min^{-1}), k_2 the second order rate constant (kg mol^{-1} min^{-1}). The model parameters: q_e, k_1, and k_2 were determined by a nonlinear regression analysis to avoid statistical bias as the pseudo-first order rate cannot be rearranged to a complete linear form while the second order rate equation can. STATISTICA Version 6.0 was employed for these nonlinear fitting of the experimental data.

2.3.3. Sorption kinetic model based on reaction mechanism

To understand the sorption mechanism, additional details from kinetic data were studied using sorption kinetic models based on mechanism. Generally the sorption includes 4 steps as follows: (1) sorbate transfers from bulk solution to boundary film, (2) sorbate transfers from the boundary film to surface of sorbent (external mass transfer step), (3) sorbate transfers from the sorbent surface to intraparticle active site or binding site (intraparticle diffusion step) and (4) sorption of the sorbate on the active or binding sites of sorbent. Steps 1 and 4 generally rapidly occur and do not consider as the rate limiting steps while the slower Steps 2 and/or 3 are mainly considered as rate limiting step(s).

The external mass transfer coefficient can be calculated from Eq. (7) [15]:

$$\frac{dq}{dt} = K_L A(C - C_s) \tag{7}$$

where K_L is the liquid–solid external mass transfer coefficient (m s^{-1}), A the specific surface area of biomass (m^2 kg^{-1}), C the liquid phase concentration of sorbate at time t in the bulk solution (mol m^{-3}), and C_s the concentration of sorbate in the inner pore of sorbent (mol m^{-3}). The parameter K_L can be determined approximately using limit theorem as

$$\lim_{t\to 0}\frac{dq}{dt} = \lim_{t\to 0} K_L A(C - C_s) \tag{8}$$

At $t=0$, C approaches C_o, and C_s approaches zero, Therefore:

$$K_L = \frac{\lim_{t\to 0}(dq/dt)}{AC_o} = \frac{h}{60AC_o} \tag{9}$$

where C_o is the initial concentration used (mol m^{-3}), h the initial sorption rate (mol kg^{-1} min^{-1}) and 60 is a conversion factor for converting the unit of h from mol kg^{-1} min^{-1} to mol kg^{-1} s^{-1}. The parameter h can be determined from the initial slope of the relationship between q and t using pseudo-first or pseudo-second order kinetic models (Eqs. (3)–(6)). Hence, h is equal to $q_e k_1$ and $q_e^2 k_2$ for the sorption that fits pseudo-first and pseudo-second kinetic models, respectively.

The specific surface area (A, m^2 kg^{-1}) can be calculated using the assumption of spherical shape sorbent where

$$A = \frac{\text{Surface Area}}{\text{Mass}} = \frac{4\pi(d_p/2)^2}{\rho_b(4/3)\pi(d_p/2)^3} = \frac{6}{\rho_b d_p} \tag{10}$$

where ρ_b is the bulk density of the biomass (kg m^{-3}) and d_p the mean particle diameter (m).

Another important mechanistic model is intraparticle diffusion Model. Generally, two models are used in the determination of intraparticle diffusion coefficient. The first model is Vermeulen model [16] which can be expressed as:

$$q = q_e\sqrt{1 - \exp\left(-\frac{4\pi^2 D_e t}{d_p^2}\right)} \tag{11}$$

where D_e is the effective diffusion coefficient (m^2 min^{-1}) and the other parameters take the same meaning as those mentioned earlier. The determination of the effective diffusion coefficients can be achieved by fitting the model with experimental data using nonlinear regressing analysis to find both q_e and D_e.

The second model is Weber and Morris sorption kinetic model [17] which can be expressed as:

$$q = I + K_{WM}\sqrt{t} \tag{12}$$

where K_{WM} is the Weber and Morris intraparticle diffusion rate (mol kg^{-1} min$^{-0.5}$), I the intercept of vertical axis (same unit with q). The determination of the two parameters can be achieved by plotting q and $\sqrt{t}$. The linear region of the curve was selected for the fitting with the model using linear regression analysis where the slope and intercept represented K_{WM} and I, respectively. The y-axis interception (sorption capacity axis) in the plot of q and $\sqrt{t}$ could be employed to examine the relative significance of the two transport mechanisms of the solute, i.e. intraparticle diffusion and external mass transfer. Should $I=0$, the intraparticle diffusion was considered as the rate limiting step, while, at $I>0$, both external mass transfer and intraparticle diffusion were considered as rate limiting step [18–20].

Crank proposed the calculation of diffusion coefficient from Weber and Morris intraparticle diffusion rate in 1975 [21] expressed as.

$$D_e = \pi\left(\frac{d_p K_{WM}}{12 q_e}\right)^2 \tag{13}$$

where D_e is the effective diffusion coefficient (m^2 min^{-1}) and the other parameters take the same meaning as those mentioned in Eqs. (4) and (11).

2.3.4. Sorption equilibrium isotherm model

The sorption isotherm is the relationship between equilibrium concentration of the solute in the solution and quantity of the solute in the sorbent at constant temperature. The data of sorption equilibrium in this work was tested with Langmuir [22] and Dubinin–Radushkevich [23] isotherm models as expressed in

Table 1
Elemental composition of zeolite (amount in % by weight)

Amount (%)	Parameter									
	Na_2O	MgO	Al_2O_3	SiO_2	P_2O_5	SO_3	K_2O	CaO	TiO_2	Fe_2O_3
CFA	0.23	0.75	21.39	43.10	0.17	0.01	3.56	0.74	0.68	5.27
Obtained Zeolite	nd	0.49	10.8	40.76	nd	0.124	1.56	3.89	1.03	9.59

nd, not detected with the accuracy of the selected analytical method.

Eqs. (14) and (15), respectively.

$$q_e = \frac{q_{max} b C_e}{1 + b C_e} \tag{14}$$

$$\left.\begin{aligned} q_e &= q_{max}\ \exp\{\beta[R_g T \ln(1 + C_e^{-1})]^2\} \\ E &= \frac{1}{\sqrt{-2\beta}} \end{aligned}\right\} \tag{15}$$

where q_e takes the same meaning as that in Eqs. (3)–(6), C_e the equilibrium concentration of the heavy metal ion in the solution (mol m^{-3}), q_{max} the maximum amount of metal ion uptaken per unit mass of the sorbent (mol kg^{-1}), b the Langmuir affinity constant (m^3 mol^{-1}), β activity coefficient (mol^2 kJ^{-2}), E the mean sorption energy (kJ mol^{-1}), R_g universal gas constant (8.314×10^{-3} kJ mol^{-1} K^{-1}) and T temperature (K). STATISTICA Version 6.0 was employed for these nonlinear parameter fittings.

3. Results and discussion

3.1. Sorbent characterization

The elemental composition analysis by XRF in Table 1 indicated that CFA contained large quantities of silica and alumina which are the two main components in zeolite. The XRD pattern in Fig. 1 suggests that the zeolite product was of X-type. The density of the obtained zeolite determined by the gas pycnometer technique was 2.10 g cm^{-3} while that of CFA was 2.24 g cm^{-3} whereas the density of the zeolite and CFA determined by the water pycnometer technique were about 2.25 and 2.42 g cm^{-3}, respectively. The particle size distribution in Fig. 2 shows that the size of zeolite fell in a range of 0.5–300 μm with an average of about 38.5 μm. The specific surface area and specific pore volume obtained from N_2-BET technique were 344 m^2 g^{-1} and 0.4921 cm^3 g^{-1}, respectively. Fig. 3 illustrates the relation between zeta potential and the pH of the solution and the results indicated that zeolite's surface had negative charge at pH higher than 3. In other words the point of zero charge or PZC was less than 3. Hence, the zeolite could be used as sorbent for positively charged contaminants such as heavy metal ions above this pH range. This finding was verified by the results on the CEC where the CEC of the obtained zeolite was about 140 meq/100 g, a significantly higher figure than 6–7 meq/100 g obtained from the original CFA.

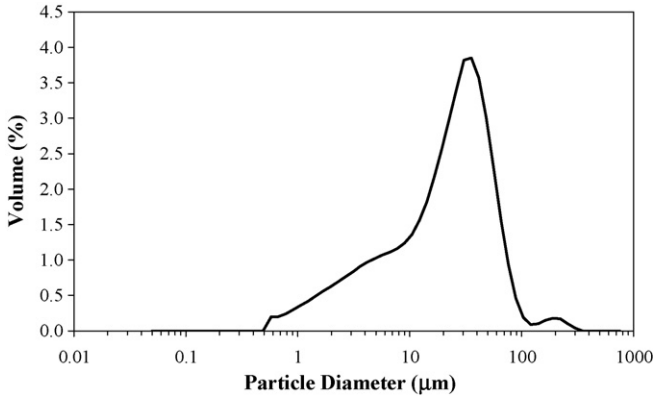

Fig. 2. Particle size distribution of zeolite.

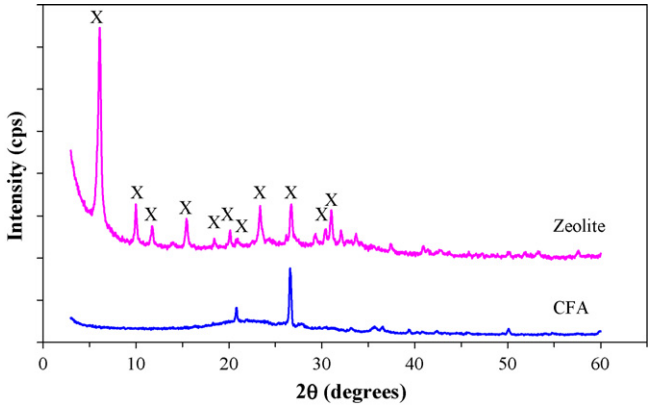

Fig. 1. XRD characteristic peak of original CFA and obtained zeolite.

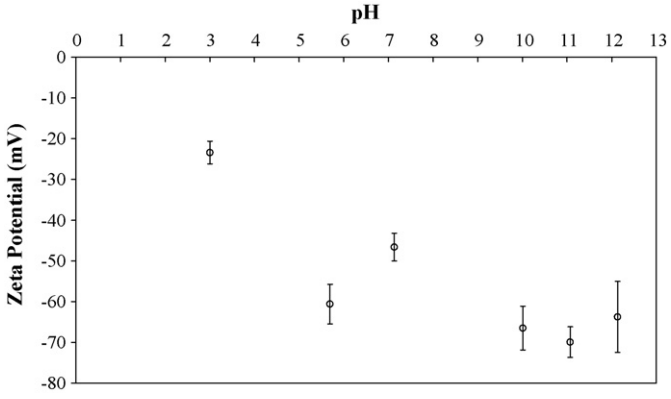

Fig. 3. Relationship between surface charge of zeolite and pH.

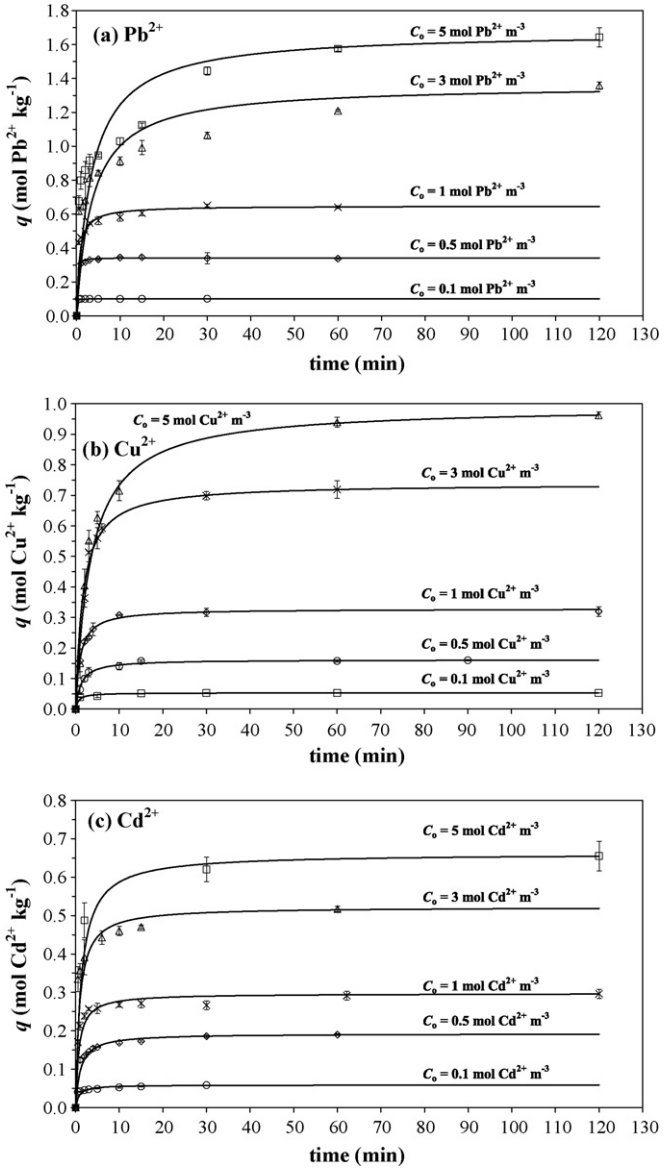

Fig. 4. Relationship between contact time and sorption capacity (q) at various concentration using sorbent dose of 1 g L^{-1}.

3.2. Effect of initial concentration and sorbent dose on sorption kinetics

The time-profiles of the sorption capacities of Pb^{2+}, Cu^{2+}, and Cd^{2+} by zeolite for a range of initial concentration from 0 to 5 mol m^{-3} and a sorbent dose of 1 g L^{-1} are given in Fig. 4. Although it took slightly longer for the systems at high initial metal concentrations to reach equilibrium than those with low initial concentration, generally the sorption reached equilibrium within 120 min. Experimental data were analyzed with the sorption kinetic models (Eqs. (4) and (6)) and the resulting parameters of each kinetic model are summarized in Table 2. This table also demonstrates that the order of equilibrium sorption capacity from both models ($q_{e,1}$ and $q_{e,2}$) increased with initial concentration. This was due to the existence of equilibrium between the liquid phase concentration and the sorption capacity of the zeolite such that an increase in the initial concentration shifted the equilibrium towards a higher sorption capacity region. On the other hand, the kinetic rate constants (k_2) were adversely affected by the initial concentration. This indicated that the systems with lower initial metal concentration reached equilibrium faster than the systems with higher initial concentration.

The pseudo-second order kinetic model was shown to be a better model for this set of experimental data than the pseudo-first order kinetic model for all cases (considered from a higher determination coefficient, R^2). Azizian and Yahyaei [24] stated that an additional criterion in the discrimination between the pseudo-first and pseudo-second order kinetic models was that the rate constant (k_1) increased with an increase in initial concentration for the pseudo-first order model while decreased if the reaction obeyed the pseudo-second order model. The experimental data from this work agreed well with their criterion, and this strongly confirmed the applicability of the second order model. Hence, the pseudo-second order kinetic model was thereafter used as a representative model in this study, and the model prediction of experimental data was plotted as solid lines in Fig. 4.

The time-profiles of the sorption capacity of Pb^{2+}, Cu^{2+}, and Cd^{2+} by zeolite for a range of sorbent dose from 0.5 to 3 g L^{-1} at an initial heavy metal concentration of 5 mol m^{-3} are provided in Fig. 5 and the parameters of each kinetic model are summarized in Table 3. Again, equilibrium was reached within 120 min and the pseudo-second order kinetic model was better than pseudo-first order kinetic models for the prediction of experimental data in all cases. The equilibrium sorption capacity decreased with an increase in the sorbent dose. This was not uncommon as an increase in the sorbent dose provided more space for the sorbate and the population of sorbate in the sorbent therefore decreased. This could also be explained using Eq. (2) as an increase in the sorbent dose increased the denominator in this equation, reducing the sorption capacity at equilibrium. In terms of k_1, no general trend could be observed from this experiment whereas the values of k_2 seemed to increase with zeolite dose. This indicated that the systems with lower sorbent dose reached equilibrium slower than the systems with higher sorbent dose. This was because an increase in the sorbent dose provided more surface area, and promoted a faster sorption.

3.3. Mechanism in sorption kinetics

Sorption kinetic models based on reaction mechanisms (Eqs. (7)–(13)) were tested for the compatibility with experimental data. Model parameters were obtained from the characterization of the zeolite product as stated in Section 3.1 and briefly summarized as follows: mean particle diameter (d_p) at approximately 3.85×10^{-5} m and bulk density (ρ_b) of 2100 kg m^{-3}. This makes a specific surface area (A) of 74.22 m^2 kg^{-1}. The other models parameters and variables were summarized in Table 4.

The results from the model as summarized in Table 4 illustrates that, the external mass transfer coefficient (K_L) from

Table 2
Sorption kinetic parameters (initial concentration range of 0–5 mol m^{-3}, sorbent dose = 1 g L^{-1})

C_o (mM)	Pseudo-first order model			Pseudo-second order model		
	$q_{e,1}$ (mol kg^{-1})	k_1 (min^{-1})	R^2	$q_{e,2}$ (mol kg^{-1})	k_2 (kg mol^{-1} min^{-1})	R^2
(a) Pb^{2+}						
0.1	0.101	13.4	1.00	0.102	237	1.00
0.5	0.337	2.35	0.995	0.343	39.4	1.00
1	0.584	2.11	0.935	0.649	2.56	1.00
3	1.07	0.615	0.778	1.36	0.205	0.994
5	1.28	0.705	0.726	1.68	0.173	0.997
(b) Cu^{2+}						
0.1	0.0502	1.53	0.962	0.0531	30.0	1.00
0.5	0.154	0.514	0.990	0.161	6.45	1.00
1	0.309	0.579	0.983	0.328	2.78	1.00
3	0.698	0.371	0.989	0.738	0.833	1.00
5	0.913	0.246	0.966	0.991	0.287	0.999
(c) Cd^{2+}						
0.1	0.0508	2.71	0.936	0.0591	23.6	0.998
0.5	0.171	0.943	0.938	0.193	4.85	1.00
1	0.266	1.80	0.977	0.297	4.61	1.00
3	0.456	2.08	0.941	0.522	2.20	0.999
5	0.651	1.05	0.979	0.661	1.20	1.00

the external mass transfer model, which was determined from parameter h (initial sorption rate) from the pseudo-second order kinetic model, inversely varied with the initial concentration for all metal ions. K_L of Pb^{2+} was considerably higher than those of Cu^{2+} and Cd^{2+} for the range of initial concentration between 0.1 and 1 mol m^{-3}, particularly at low initial concentration range (e.g. at 0.1 and 0.5 mol m^{-3}) where the difference was as high as two order of magnitude (about 100 times larger). However, the effect of sorbent dose on the mass transfer coefficient differed for each metal ion. For Pb^{2+} and Cd^{2+} K_L increased gradually with the sorbent dose reaching the maximum value at approximately 2.9×10^{-5} and 3.2×10^{-5} m s^{-1}, respectively. On the other hand, K_L for Cu^{2+} seemed to be constant at 1.24×10^{-5} m s^{-1} regardless of the sorbent dose.

The results from the Vermeulen model on the equilibrium sorption capacity ($q_{e,v}$) provided a similar trend with that calculated from the pseudo-second order kinetic model, and the accuracy of the prediction from the Vermeulen model was reasonably high with the determination coefficient (R^2) of more than 0.836. The calculation revealed that the effective diffusion coefficient ($D_{e,v}$) for Pb^{2+} and Cu^{2+} decreased with an increase in the initial concentration while the trend for Cd^{2+} could not be defined. On the other hand, an increase in the sorbent dose from 0.5 to 3 g L^{-1} resulted in an enhancing Vermeulen effective diffusion coefficient of Pb^{2+}. No general trend for the effect of sorbent dose on the effective diffusion coefficient of Cu^{2+} was observed, whereas a parabolic trend for Cd^{2+} with the maximum obtained at the sorbent dose of 2 g L^{-1} was obtained.

Table 3
Sorption kinetic parameters (sorbent dose range of 0.5–3 g L^{-1}, initial concentration = 5 mol m^{-3})

X_o (g L^{-1})	Pseudo-first order model			Pseudo-second order model		
	$q_{e,1}$ (mol kg^{-1})	k_1 (min^{-1})	R^2	$q_{e,2}$ (mol kg^{-1})	k_2 (kg mol^{-1} min^{-1})	R^2
(a) Pb^{2+}						
0.5	1.97	0.705	0.818	2.31	0.0898	0.976
1	1.28	0.705	0.726	1.68	0.173	0.997
2	1.11	1.45	0.825	1.37	0.348	0.999
3	1.04	1.76	0.852	1.26	0.425	0.999
(b) Cu^{2+}						
0.5	0.950	0.362	0.938	1.07	0.246	0.992
1	0.913	0.246	0.966	0.991	0.287	0.999
3	0.550	1.38	0.807	0.706	0.538	0.996
(c) Cd^{2+}						
0.5	0.619	0.857	0.804	0.753	0.540	0.999
1	0.651	1.05	0.979	0.661	1.20	1.00
2	0.512	2.26	0.879	0.595	1.93	0.995
3	0.530	1.13	0.974	0.576	2.12	1.00

Table 4
Sorption kinetic parameters based on reaction mechanism

Metal ion	C_o (mol m^{-3})	X_o (g L^{-1})	External mass transfer model		Vermeulen model			Weber–Morris model			
			$h = q_e^2 k_2$(mol kg^{-1} min^{-1})	K_L (m s^{-1})	$q_{e,v}$ (mol kg^{-1})	$D_{e,v}$ (m^2 s^{-1})	R^2	K_{WM} (mol kg^{-1} min$^{-0.5}$)	$D_{e,WM}$ (m^2 s^{-1})	I (mol kg^{-1})	RC (%)
Pb^{2+}	0.105	1	2.45	5.25×10^{-3}	0.101	7.51×10^{-12}	1.000	2.32×10^{-4}	2.82×10^{-18}	0.100	98.5
	0.485	1	4.63	2.14×10^{-3}	0.338	1.01×10^{-12}	0.996	1.64×10^{-2}	1.23×10^{-15}	0.296	86.3
	1.02	1	1.08	2.38×10^{-4}	0.598	6.13×10^{-13}	0.957	2.76×10^{-2}	9.74×10^{-16}	0.499	76.9
	3.05	1	0.380	2.80×10^{-5}	1.13	1.48×10^{-13}	0.868	5.96×10^{-2}	1.03×10^{-15}	0.739	54.3
	5.08	1	0.485	2.14×10^{-5}	1.44	1.02×10^{-13}	0.836	1.06×10^{-1}	2.17×10^{-15}	0.708	42.3
	5.23	0.5	0.479	2.06×10^{-5}	2.32	2.23×10^{-13}	0.938	2.74×10^{-1}	7.61×10^{-15}	0.388	16.8
	5.22	2	0.655	2.82×10^{-5}	1.17	2.98×10^{-13}	0.939	9.15×10^{-2}	2.40×10^{-15}	0.725	52.8
	5.18	3	0.679	2.94×10^{-5}	1.08	4.12×10^{-13}	0.888	7.44×10^{-2}	1.87×10^{-15}	0.726	57.4
Cu^{2+}	0.101	1	0.0845	1.88×10^{-4}	0.0504	5.47×10^{-13}	0.964	4.12×10^{-3}	3.25×10^{-15}	0.0345	64.9
	0.500	1	0.168	7.52×10^{-5}	0.157	1.48×10^{-13}	0.988	7.86×10^{-2}	1.27×10^{-13}	-0.0142	-8.80
	0.970	1	0.300	6.94×10^{-5}	0.317	1.82×10^{-13}	0.998	9.97×10^{-2}	4.97×10^{-14}	0.0655	20.0
	3.04	1	0.454	3.35×10^{-5}	0.711	1.22×10^{-13}	0.991	2.00×10^{-1}	3.97×10^{-14}	0.0753	10.2
	5.10	1	0.282	1.24×10^{-5}	0.951	6.00×10^{-14}	0.967	1.61×10^{-1}	1.42×10^{-14}	0.0603	6.09
	4.96	0.5	0.279	1.26×10^{-5}	0.977	9.45×10^{-14}	0.972	2.88×10^{-1}	4.01×10^{-14}	0.0776	7.34
	4.85	3	0.268	1.24×10^{-5}	0.590	2.67×10^{-13}	0.868	7.55×10^{-2}	6.17×10^{-15}	0.312	44.3
Cd^{2+}	0.083	1	0.0825	2.24×10^{-4}	0.0518	8.66×10^{-13}	0.948	6.45×10^{-3}	6.41×10^{-15}	0.0362	61.2
	0.479	1	0.180	8.44×10^{-5}	0.177	2.77×10^{-13}	0.969	2.86×10^{-2}	1.19×10^{-14}	0.0949	49.3
	0.953	1	0.407	9.60×10^{-5}	0.271	5.74×10^{-13}	0.989	8.04×10^{-2}	4.04×10^{-14}	0.122	41.6
	2.82	1	0.599	4.77×10^{-5}	0.466	6.35×10^{-13}	0.962	6.12×10^{-2}	7.39×10^{-15}	0.296	56.7
	4.80	1	0.524	2.47×10^{-5}	0.664	3.54×10^{-13}	0.993	1.35×10^{-1}	2.03×10^{-14}	0.338	48.7
	4.89	0.5	0.306	1.4×10^{-5}	0.675	1.25×10^{-13}	0.884	8.24×10^{-2}	6.45×10^{-15}	0.279	37.0
	4.91	2	0.684	3.13×10^{-5}	0.528	6.08×10^{-13}	0.900	3.67×10^{-2}	1.86×10^{-15}	0.372	59.5
	4.95	3	0.704	3.20×10^{-5}	0.540	3.29×10^{-13}	0.988	2.33×10^{-1}	8.78×10^{-14}	0.108	18.8

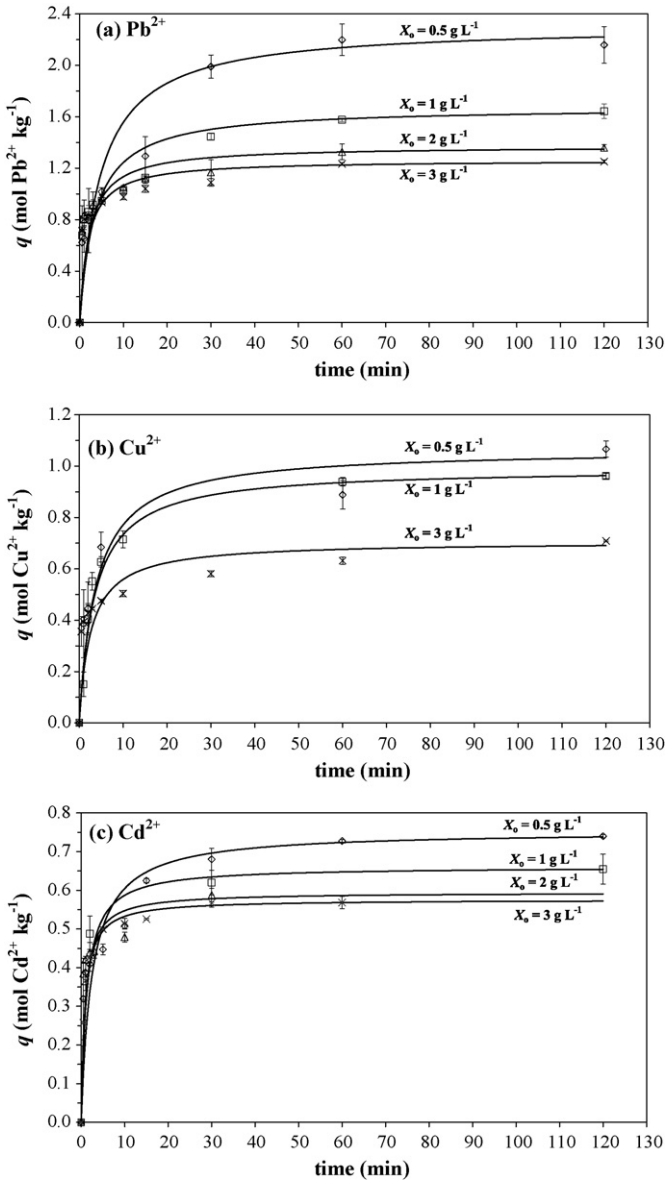

Fig. 5. Relationship between contact time and sorption capacity (q) at various sorbent dose using initial concentration of 5 mol m^{-3}.

The Weber–Morris model often predicted higher effective diffusion coefficient ($D_{e,WM}$) than those from the Vermeulen model, and in particular, the trend of $D_{e,WM}$ did not follow the same trend as that of $D_{e,v}$. This could be because $D_{e,WM}$ was determined using only the linear region which, on the one hand, depended on the judgment of the "linear region", and this might induce statistical bias. Hence, for this work, the Vermeulen model was recommended for the determination of effective diffusion coefficient. However, the Weber–Morris model still was useful in the examination of the dominant transport mechanism between external mass transfer and intraparticle diffusion. As described in Section 2.3.3, the intercept (I) of the plot between q and $\sqrt{t}$ provided an insight evaluation of the relative significance of the external mass transfer step. However, only an intercept value might not be enough as a criterion in the investigation of rate limiting step as it only gives the information on the magnitude of external mass transfer without taking into account the intraparticle diffusion. The equilibrium sorption capacity should then be incorporated with the intercept to allow a better examination, and this, in this work, was proposed as a parameter, "relative coefficient (RC)", which is expressed as the ratio between the intercept (I) and the equilibrium sorption capacity as follows:

$$\mathrm{RC}(\%) = 100 \times \frac{I}{q_e} \tag{16}$$

where I takes the same meaning as Eq. (12) and q_e the equilibrium sorption capacity obtained from the best fitted kinetic model. The higher RC would indicate the external mass transfer step as a rate limiting step, whereas the lower RC indicated that the intraparticle diffusion step was the rate limiting step. In this work, q_e from the pseudo-second order kinetic model was applied in Eq. (16) and RCs from the various experiments were reported in Table 4. It can be seen from the table that an increase in the initial concentration generally resulted in a decrease in RC for Pb^{2+}. This indicated that the external mass transfer was more significant as a rate limiting step particularly at low than high initial concentrations. RC for Cu^{2+} also decreased with an increase initial concentration, but the value of RC was mostly lower than 50%. This suggested that the sorption of Cu^{2+} was controlled primarily by intraparticle diffusion. For Cd^{2+}, no general trend could be concluded on the determination of rate limiting step and RC took the values between about 40–60%. An increase in the sorbent dose from 0.5 to 3 g L^{-1} increased RC of Pb^{2+} indicating that the external mass transfer became more significant at higher sorbent dose. The effect of sorbent dose on the rate controlling mechanism could not be clearly observed for Cu^{2+}, but the external mass transfer seemed to be more important at higher initial concentration. The relationship between RC and sorbent dose for the sorption Cd^{2+} was found to be parabolic with the maximum taken place at the sorbent dose of 2 g L^{-1}. It should be noted that the negative value of I and RC for Cu^{2+} at $C_o = 0.5$ mol m^{-3} occurred as the linear regression in calculation of K_{WM} resulted in the y-intercept below horizontal axis. The reason could be that the process was highly limited by intraparticle diffusion step.

In conclusion, the sorption of Pb^{2+} was often controlled by the external mass transfer process (RC always higher than 50%). On the other hand, the sorption of Cu^{2+} was generally found to involve with the intraparticle diffusion process (RC always lower than 50%). The sorption on Cd^{2+} seemed to involve equally the external mass transfer and the intraparticle diffusion as RC generally varied in a range of 40–60%.

The reason for different rate limiting steps could be due to the different sizes of metal ions which are related to the atomic weight. Wilke–Chang (1955) proposed the relationship between diffusion coefficient (D) and the molecular weight (M_w) as follows: $D = 7.4 \times 10^{-8} T\sqrt{M_w}/\eta V^{0.6}$ [25]. This indicated that lower molecular weight molecules exhibited lower diffusion coefficient. In this work, Cu^{2+} has the lowest atomic weight and therefore it was expected to have the lowest diffusion coefficient. As a result, the intra-particle diffusion for Cu^{2+} could be more limiting when compared to other metal ions.

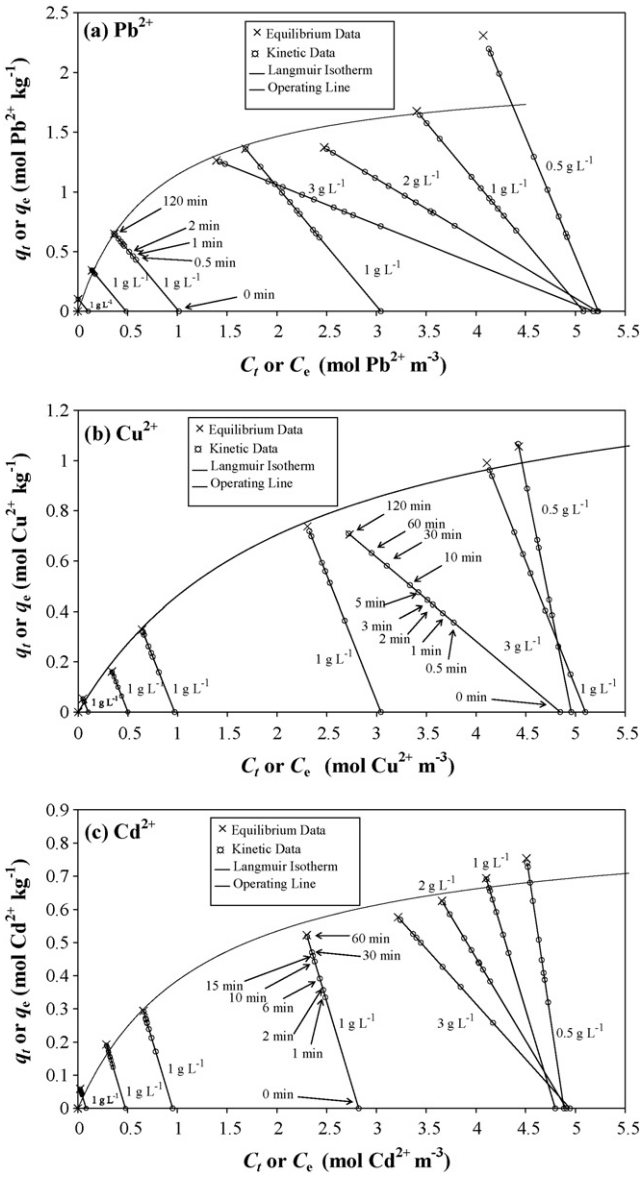

Fig. 6. Sorption isotherm with kinetic tracking plots.

3.4. Sorption isotherm

The sorption equilibrium curve was constructed from the kinetic data with sufficient contact time as shown in Fig. 6. As the contact time increased, the bulk liquid phase concentration (C_t) decreasingly converged to equilibrium bulk liquid phase concentration (C_e), and solid phase concentration or the sorption capacity (q_t) increasingly converged to equilibrium sorption capacity (q_e). The liquid phase concentration at time t (C_t) and equilibrium concentration (C_e) can be calculated by rearranging Eq. (2) as follows:

$$C_t = C_o - \frac{mq_t}{V} \tag{17a}$$

$$C_e = C_o - \frac{mq_e}{V} \tag{17b}$$

Each experiment provided a dot line with the final point lied on the equilibrium line as illustrated in Fig. 6. Each equilibrium data were fitted with the isotherm models, Eqs. (14) and (15), and the isotherm parameters are summarized in Table 5.

Langmuir isotherm suggested that the order of maximum sorption capacity (q_{max}) could be prioritized from high to low as: $Pb^{2+} > Cu^{2+} > Cd^{2+}$, indicating that the zeolite product from this work had more binding sites for Pb^{2+} than Cu^{2+} and Cd^{2+}, respectively. On the other hand, the Langmuir affinity constant (b) could be prioritized from high to low as: $Pb^{2+} > Cd^{2+} > Cu^{2+}$ which suggested that Pb^{2+} was the most easily bonded component to the binding sites of the zeolite, followed by Cd^{2+} and Cu^{2+}, respectively.

The Dubinin–Radushkevich isotherm model was employed to evaluate the energy of sorption. The analysis from Dubinin–Radushkevich isotherm showed that the mean sorption energies were 2.55, 1.57, and 2.05 kJ mol^{-1} for Pb^{2+}, Cu^{2+}, and Cd^{2+}, respectively. Smith [26] illustrated that the range of energy of sorption at 2–20 kJ mol^{-1} could be considered physisorption in nature. Therefore, it was possible that physical means such as electrostatic force played a significant role as a sorption mechanism for the sorption of heavy metal ions in this work.

3.5. Effect of sorbent dose and initial concentration on sorption equilibrium

The effect of sorbent dose and initial concentration on equilibrium study is important in designing the treatment unit, and the relationships between these parameters were often constructed. For example, on the investigation of the sorption of nickel ions on baker yeast, Padmavathy et al. [27] proposed the relationship between equilibrium sorption capacity and initial metal concentration as: q_e (in mg g^{-1}) = C_o (in mg L^{-1})/$8.95 \times 10^{-2}\, C_o + 3.57$ for sorbent dose 1 g L^{-1} and the relationship between sorption capacity and sorbent dose as: q_e(in mg g^{-1}) = $7.15\, m_s^{-0.686}$(in g L^{-1}) for initial concentration about 100 mg L^{-1}. Kumar and Kumaran [28], who studied the removal of Methylene blue by mango seed kernel powder, suggested the relationship between equilibrium sorption capacity and initial dye concentration

Table 5
Sorption isotherm parameters

Metal ion	Langmuir isortherm			Dubinin–Radushkevich isotherm			
	q_{max} (mol kg^{-1})	b (m^3 mol^{-1})	R^2	q_{max} (mol kg^{-1})	β (mol^2 kJ^{-2})	E (kJ mol^{-1})	R^2
Pb^{2+}	2.03	1.29	0.994	1.61	−0.0770	2.55	0.970
Cu^{2+}	1.43	0.468	0.993	0.989	−0.203	1.57	0.974
Cd^{2+}	0.870	0.797	0.980	0.640	−0.119	2.05	0.923

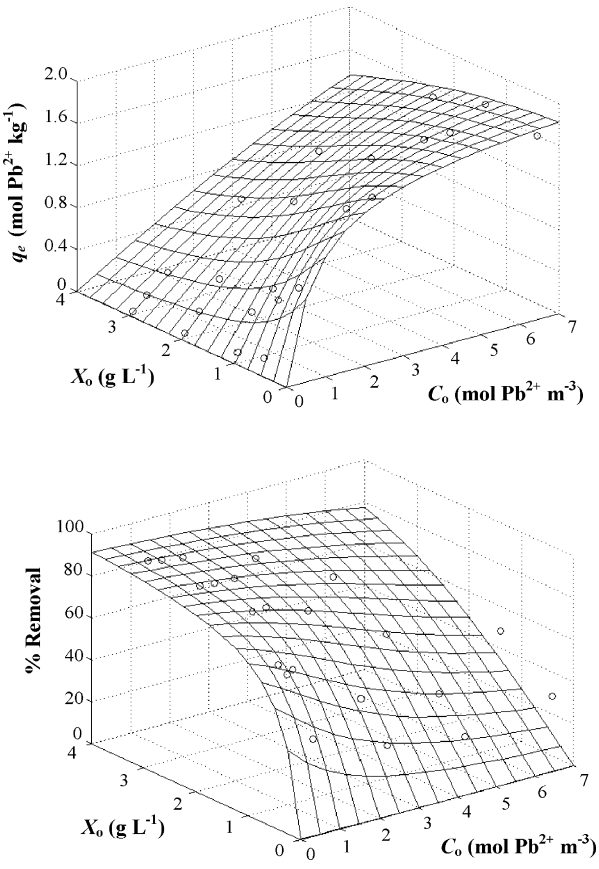

Fig. 7. Relationship between sorption parameters (q_e and %Removal) of Pb^{2+} and operating parameters (C_o and X_o).

as: $q_e = 0.4167C_o^2 + 4.0086C_o/0.5833C_o - 4.0086$ for sorbent dose 0.6 g L^{-1}, while the relationship between the q_e and adsorbent mass fitted with: m(in g) = $0.0003q_e$(in mg g^{-1})/$0.0242q_e - 1$ for an initial dye concentration of 100 mg L^{-1}. Suthiparinyanont et al. [29] observed that the sorption capacity for Cu^{2+}, Cd^{2+}, and Pb^{2+} increased with an increase in initial metal concentration, except for Zn^{2+} where an increase in initial concentration from 1 to 1.5 mol m^{-3} led to a slower rate of change in the sorption capacity. Ho and Ofomaja [30] reported that the relationship between coconut copra meal dose and %Removal of initial concentration about 128 mg-Cd^{2+} L^{-1} (1.14 mol Cd^{2+} m^{-3}) could be fitted by; %Removal = m_s (in g L^{-1})/$7.97 \times 10^{-2} + 1.60 \times 10^{-2}$ m_s, while the relationship between the sorbent dose and sorption capacity was: q_e (in mg g^{-1}) = $1/6.20 \times 10^{-2} + 1.25 \times 10^{-2}$ m_s (in g L^{-1}).

In this work, the effect of sorbent dose (X_o) and initial concentration (C_o) was found to simultaneously control the equilibrium parameters such as equilibrium sorption capacity (q_e) and removal percentage (%Removal). The relationship between these parameters could be achieved by combining Eqs. (14) and (17b) where m/V is defined as X_o, and this leads to:

$$q_e = \frac{q_{max} b(C_o - X_o q_e)}{1 + b(C_o - X_o q_e)} \tag{18}$$

In this equation, X_o represents sorbent dose (g L^{-1} or kg m^{-3}) and the other parameters take the same meaning as those in Eqs. (2) and (14). Rearranging Eq. (18) gives:

$$(bX_o)q_e^2 - (1 + bC_o + q_{max}bX_o)q_e + (q_{max}bC_o) = 0 \tag{19}$$

The above equation is quadratic and therefore the solutions can be obtained from:

$$q_e = \frac{(q_{max}bX_o + bC_o + 1) \pm \sqrt{b^2C_o^2 + 2b(1 - q_{max}bX_o)C_o + (1 + q_{max}bX_o)^2}}{2bX_o} \tag{20}$$

As $q_e = 0$ when $C_o = 0$, if the operation between the two terms was "plus", the substitution of C_o with zero gives: $q_e = (q_{max}bX_o + 1)/bX_o$ which was not equal to zero. Hence, the operation must be negative and the actual exact solution of Eq. (19) can be expressed as:

$$q_e = \frac{(q_{max}bX_o + bC_o + 1) - \sqrt{b^2C_o^2 + 2b(1 - q_{max}bX_o)C_o + (1 + q_{max}bX_o)^2}}{2bX_o} \tag{21}$$

With this information, the determination the effect of initial concentration and sorbent dose on removal percentage can also be achieved by combining Eqs. (1) and (2) where q, C_f, and m/V were substituted by q_e, C_e, and X_o, respectively. This results in:

$$\%\text{Removal} = 100\frac{q_e X_o}{C_o} \tag{22}$$

In this equation, %Removal represents the removal percentage at equilibrium. The other parameters take the same meaning as those in Eqs. (2) and (18). Substitution of q_e from Eq. (21) into Eq. (22) gives:

$$\left(\%\text{Removal} = 50\frac{(q_{max}bX_o + bC_o + 1) - \sqrt{b^2C_o^2 + 2b(1 - q_{max}bX_o)C_o + (1 + q_{max}bX_o)^2}}{bC_o}\right) \tag{23}$$

3.6. Model verification

New sets of sorption experiments were carried out to verify the models in Eqs. (21) and (23). It should be noted that the contact time of about 2 h were assumed, from experience in Section 3.2, to be adequate for the system to reach equilibrium. The results from the experiments along with the model predictions were compared as illustrated in Figs. 7–9 for Pb^{2+}, Cu^{2+}, and Cd^{2+}, respectively.

Parameters employed to verify the model prediction were: (i) the coefficient of determination (R^2), (ii) average of %Error, and (iii) relative standard deviation (R.S.D.) of %Error. These

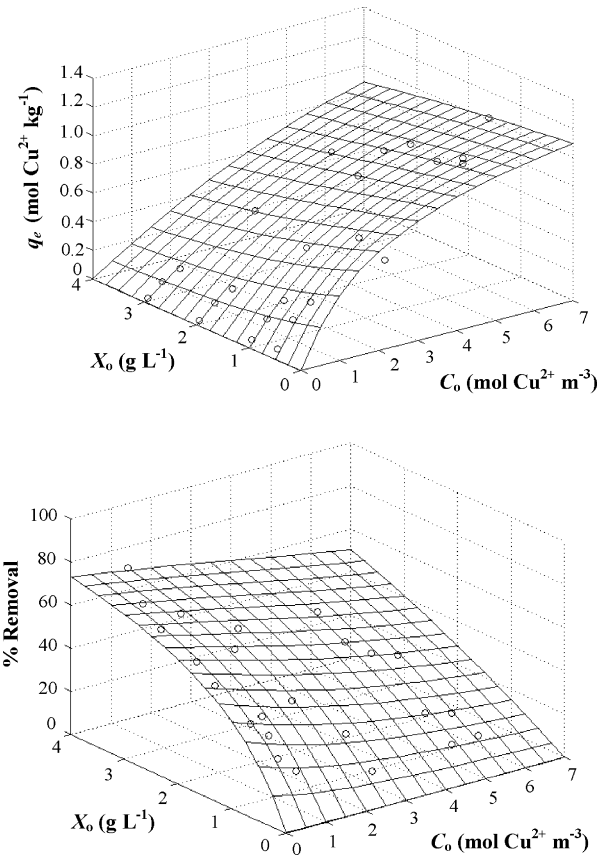

Fig. 8. Relationship between sorption parameters (q_e and %Removal) of Cu^{2+} and operating parameters (C_o and X_o).

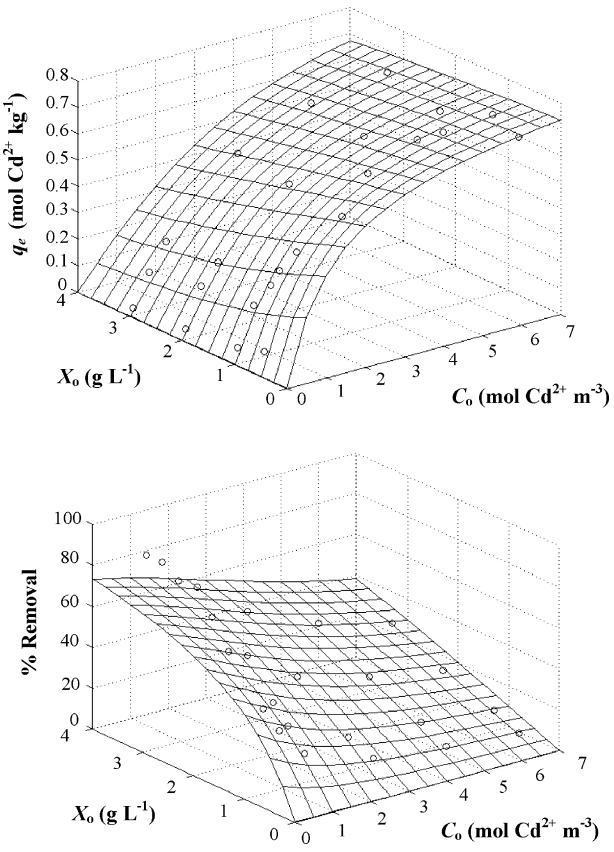

Fig. 9. Relationship between sorption parameters (q_e and %Removal) of Cd^{2+} and operating parameters (C_o and X_o).

are calculated from:

$$R^2 = 1 - \frac{\sum_{i=1}^{N}(y_i - y_{c,i})^2}{\sum_{i=1}^{N}(y_i - \bar{y})^2} \tag{24a}$$

$$E_i = \left| \frac{y_i - y_{c,i}}{y_i} \right| \tag{24b}$$

$$\text{Average of Error } (\%) = \frac{100 \times \sum_{i=1}^{N} E_i}{N} \tag{24c}$$

$$\text{R.S.D. of Error } (\%) = 100 \times \sqrt{\frac{\sum_{i=1}^{N}(E_i - \bar{E})^2}{N\bar{E}^2}} \tag{24d}$$

where y_i is the actual model variables (can be either q_e or %Removal) at point i obtained from experimental data, $y_{c,i}$ the predicted actual model variables from the model at the same point as y_i, $\bar{y}$ the average of actual model variables from all interested experimental data, E_i the error at point i, $\bar{E}$ the average of error from all experimental data, and N the number of experimental data.

Table 6
Parameters for model verification

Variables	Metal	R^2	Average error (%)	R.S.D.[a] of error (%)	Max error (%)	Min error (%)	%Data that error less than 10%	No. of data
q_e	Pb^{2+}	0.928	14.7	64.0	31.0	0.303	37.5	24
	Cu^{2+}	0.872	22.9	95.6	79.8	0.893	37.5	24
	Cd^{2+}	0.922	19.0	77.2	52.7	0.632	33.3	24
	All Data	0.929	18.9	86.3	79.8	0.303	36.1	72
%Removal	Pb^{2+}	0.821	14.7	64.0	31.0	0.303	37.5	24
	Cu^{2+}	0.672	22.9	95.6	79.8	0.893	37.5	24
	Cd^{2+}	0.704	19.0	77.2	52.7	0.632	33.3	24
	All Data	0.783	18.9	86.3	79.8	0.303	36.1	72

[a] R.S.D. = relative standard deviation = 100 × standard deviation/average.

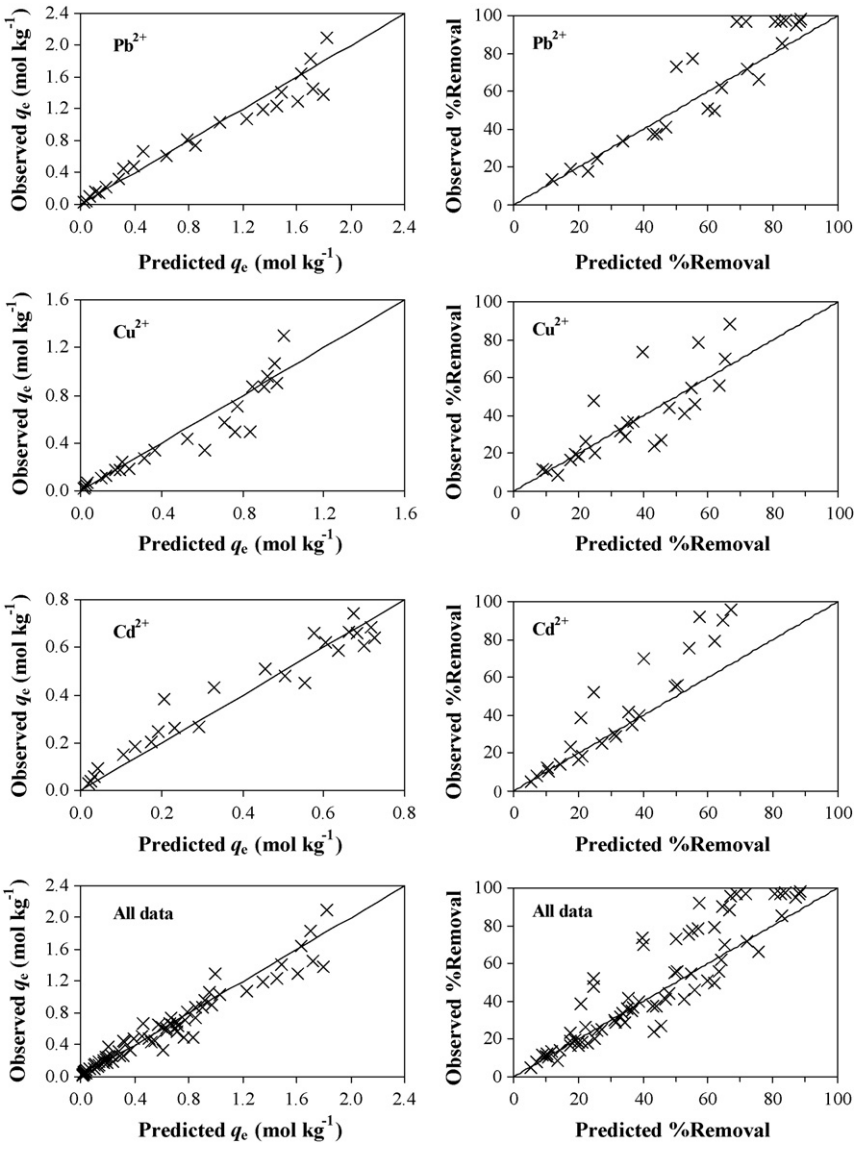

Fig. 10. Accuracy of the models prediction.

The parameters for model verification are shown in Table 6 whereas the accuracy of the models is plotted in the Fig. 10. A high R^2, low average of percentage error (Average of %Error), and low relative standard deviation of percentage error (R.S.D. of %Error) indicated high accuracy of the model in the prediction of sorption characteristics. Note that the model could predict the sorption performance for Pb^{2+} and Cd^{2+} better than that of Cu^{2+}.

4. Conclusions

The sorption of three heavy metal ions, i.e. Pb^{2+}, Cu^{2+}, and Cd^{2+} using zeolite X modified from coal fly ash was evaluated here. Sorption kinetic mechanism was analyzed and found that generally both external mass transfer and intraparticle diffusion are the rate limiting step for Pb^{2+} and Cd^{2+} while Cu^{2+} seemed to generally be governed by intraparticle diffusion. The maximum sorption capacity (q_{max}) of the metal ions calculated from Langmuir isotherms was always higher than that reported in literature (Table 7) indicating that zeolite from this work could well be used as a high performance sorbent in sequestering of contaminated metals in wastewater. A general mathematical model for predicting the sorption parameters (q_e and %Removal) was proposed. The model could simultaneously integrate the effects of initial concentration and sorbent dose, and provide a relatively accurate prediction of sorption and this is applicable for further reference. Overall, this work illustrates the possibility in the conversion of the unwanted industrial materials such as coal fly ash from power plants to a high performance zeolite sorbent which could be useful for the removal of heavy metal ions from the wastewater.

Table 7
Maximum sorption capacities for heavy metals of various sorbents

Sorbent	q_{max} (mol kg^{-1})	pH	Reference
S. cinnamoneum	Pb(0.36) > Cd(0.19) > Cu(0.14)	4.0	[31]
P. chrysogenum	Pb(0.34) > Cu(0.20) > Cd(0.11)	4.0	[31]
Durvillaea potatorum	Pb(1.55) > Cu(1.30)	5.0	[32]
Ecklonia radiata	Pb(1.26) > Cu(1.11)	5.0	[32]
Aspergillus niger	Cu(0.073) > Pb(0.049) > Cd(0.035)	5.0	[33]
Sphaerotilus natans	Pb(0.65) = Cu(0.65) > Cd(0.23)	5.0	[34]
Bone char	Cu(0.709) > Cd(0.477)	5.0	[35]
Pine bark	Cu(0.149) > Cd(0.126)	[a]	[36]
Chlorella vulgaris	Pb(0.816)	5.0	[37]
Caulerpa lentillifera	Pb(0.14) > Cu(0.13) > Cd(0.042)	5.0	[38]
Rice husk ash	Pb(0.061)	5.6–5.8	[39]
Cymodocea nodosa	Cu(0.83)	4.5	[40]
Padina sp.	Cu(0.80)	5.0	[41]
GAC[b]	Cu(0.043) > Cd(0.0219)	5.4–5.7	[42]
Modified GAC by Citric â	Cu(0.235)	4.9	[43]
Sepiolite	Cd(0.152)	6.0	[44]
Zeolite Na-P1	Pb(1.29) > Cu(1.05) > Cd(1.16)	[a]	[6]
Zeolite faujasite	Pb(1.23)	[a]	[6]
Zeolite sodalite	Pb(0.798)	[a]	[6]
Zeolite analcime	Pb(0.745)	[a]	[6]
Zeolite cancrinite	Pb(0.537)	[a]	[6]
Zeolite clinoptilolite	Cu(1.41)	6–7	[7]
Zeolite clinoptilolite	Cu(0.405) > Pb(0.130) > Cd(0.043)	6.2	[45]
Zeolite X	Pb(2.03) > Cu(1.43) > Cd(0.870)	5.0	This work

[a] Not defined.
[b] Granular activated carbon.

Acknowledgements

The authors wish to acknowledge the Thailand Research Fund (Royal Golden Jubilee Ph.D. Scholarship) for the financial support and National Power Supply Co. Ltd. (Thailand) for providing the Coal Fly Ash used in the study.

References

[1] M. Sebastiá, I.F. Olmo, A. Irabien, Neural network prediction of unconfined compressive strength of coal fly ash–cement mixtures, Cement Concrete Res. 33 (8) (2003) 1137–1146.
[2] V.S. Somerset, L.F. Petrik, R.A. White, M.J. Klink, D. Key, E.I. Iwuoha, Alkaline hydrothermal zeolites synthesized from high SiO_2 and Al_2O_3 co-disposal fly ash filtrates, Fuel 84 (18) (2005) 2324–2329.
[3] W.H. Shih, H.L. Chang, Conversion of fly ash into zeolites for ion-exchange applications, Mater. Lett. 28 (4–6) (1996) 263–268.
[4] A. Rujiwatra, M. Phueadpho, K. Grudpan, Selective synthesis of zeolitic phillipsite and hibschite hydrogarnet from lignite ash employing calcium hydroxide under mild conditions, J. Phys. Chem. Solids 66 (2005) 1085–1090.
[5] A. Molina, C. Poole, A comparative study using two methods to produce zeolites from fly ash, Miner. Eng. 17 (2) (2004) 167–173.
[6] M.G. Lee, G. Yi, B.J. Ahn, F. Roddick, Conversion of coal fly ash into zeolite and heavy metal removal characteristics of the products, Korean J. Chem. Eng. 17 (3) (2000) 325–331.
[7] E. Erdem, N. Karapinar, R. Donat, The removal of heavy metal cations by natural zeolites, J. Colloid Interface Sci. 280 (2004) 309–314.
[8] http://www.epa.gov/epaoswer/hazwaste/test/pdfs/9081.pdf.
[9] S. Lagergren, Zur Theorie der sogenannten adsorption gelöster stoffe, Kungliga Svenska Vetenskapsakademiens Handlingar 24 (4) (1898) 1–39.
[10] G. Blanchard, M. Maunaye, G. Martin, Removal of heavy-metals from waters by means of natural zeolites, Water Res. 18 (1984) 1501–1507.
[11] J. Sobkowsk, A. Czerwiński, Kinetics of carbon dioxide adsorption on a platinum electrode, J. Electroanal. Chem. 55 (1974) 391–397.
[12] Y.S. Ho, Adsorption of heavy metals from waste streams by peat, Ph.D. Thesis, University of Birmingham, Birmingham, UK, 1995.
[13] S. Azizian, Kinetic models of sorption: a theoretical analysis, J. Colloid Interface Sci. 276 (2004) 47–52.
[14] W. Rudzinski, W. Plazinski, Kinetics of solute adsorption at solid/solution interfaces: a theoretical development of the empirical pseudo-first and pseudo-second order kinetic rate equations, based on applying the statistical rate theory of interfacial transport, J. Phys. Chem. B 110 (2006) 16514–116514.
[15] R. Apiratikul, P. Pavasant, Batch and column studies of biosorption of heavy metals by *Caulerpa lentillifera*, Bioresour. Technol. 99 (2008) 2766–2777.
[16] T. Vermeulen, Theory for irreversible and constant pattern solid diffusion, Ind. Eng. Chem. Res. 45 (8) (1953) 1664–1670.
[17] W.J. Weber, J.C. Morris, Advance in water pollution research: removal of biological resistant pollutions from wastewater by adsorption, in: Proceedings of the International Conference on Water Pollution Symposium, Pergamon Press, Oxford, 1962.
[18] B. Acemioglu, Batch kinetic study of sorption of methylene blue by perlite, Chem. Eng. J. 106 (2004) 73–81.
[19] M.H. Kalavathy, T. Karthikeyan, S. Rajgopal, L.R. Miranda, Kinetic and isotherm studies of Cu(II) adsorption onto $H_3PO_4^-$ activated rubber wood sawdust, J. Colloid Interface Sci. 292 (2) (2005) 354–362.
[20] J. Shen, Z. Duvnjak, Adsorption kinetics of cupric and cadmium ions on corncob particles, Process Biochem. 40 (11) (2005) 3446–3454.
[21] J. Crank, The Mathematics of Diffusion, second ed., Clarendon, Oxford, 1975.
[22] I. Langmuir, The sorption of gases on plane surfaces of glass, mica and platinum, J. Am. Chem. Soc. 40 (1918) 1361–1403.
[23] M.M. Dubinin, L.V. Radushkevich, Equation of the characteristic curve of activated charcoal, Chemisches Zentralblatt 1 (1947) 875–889.

[24] S. Azizian, B. Yahyaei, Adsorption of 18-crown-6 from aqueous solution on granular activated carbon: a kinetic modeling study, J. Colloid Interface Sci. 299 (1) (2006) 112–115.
[25] C.R. Wilke, P. Chang, Correlation of diffusion coefficients in dilute solutions, AlChE J. 1 (2) (1955) 264–270.
[26] J.M. Smith, Chemical Engineering Kinetics, McGraw-Hill, New York, 1981.
[27] V. Padmavathy, P. Vasudevan, S.C. Dhingra, Biosorption of nickel(II) ions on Baker's yeast, Process Biochem. 38 (10) (2003) 1389–1395.
[28] K.V. Kumar, A. Kumaran, Removal of methylene blue by mango seed kernel powder, Biochem. Eng. J. 27 (1) (2005) 83–93.
[29] P. Suthiparinyanont, S. Wattanachira, T.F. Marhaba, P. Pavasant, Pretreatment of *Caulerpa lentillifera* with NaOH for biosorption of Cu, Cd, Pb and Zn, J. Thai Environ. Eng. 20 (1) (2006) 11–23.
[30] Y.S. Ho, A.E. Ofomaja, Biosorption thermodynamics of cadmium on coconut copra meal as biosorbent, Biochem. Eng. J. 30 (2) (2006) 117–123.
[31] P.R. Puranik, K.M. Paknikar, Influence of co-cations on biosorption of lead and zinc—a comparative evaluation in binary and multimetal systems, Bioresour. Technol. 70 (1999) 269–276.
[32] T.J. Matheickal, Q. Yu, Biosorption of lead(II) and copper(II) from aqueous solution by pre-treated biomass of Australian marine algae, Bioresour. Technol. 69 (1999) 223–229.
[33] A. Kapoor, T. Viraragharan, R.D. Cullimore, Removal of heavy metals using the fungus *Aspergillus niger*, Bioresour. Technol. 70 (1999) 95–104.
[34] F. Pagnanelli, M. Trifonia, F. Beolchini, A. Espositoc, L. Toroa, F. Vegliò, Equilibrium biosorption studies in single and multi-metal systems, Process Biochem. 37 (2001) 115–124.
[35] D.C.K. Ko, C.W. Cheung, K.K.H. Choy, J.F. Porter, G. McKay, Sorption equilibria of metal ions on bone char, Chemosphere 54 (2004) 273–281.
[36] S. Al-Asheh, F. Banat, R. Al-Omari, Z. Duvnjak, Predictions of binary sorption isotherms for the sorption of heavy metals by pine bark using single isotherm data, Chemosphere 41 (2000) 659–665.
[37] M.H. El-Naas, F.A. Al-Rub, I. Ashour, M.A. Marzouqi, Effect of competitive interference on the bio-sorption of lead (II) by *Chlorella vulgaris*, Chem. Eng. Process. 46 (12) (2007) 1391–1399.
[38] R. Apiratikul, P. Pavasant, Sorption isotherm model for binary component sorption of copper, cadmium, and lead ions using dried green macroalga, *Caulerpa lentillifera*, Chem. Eng. J. 119 (2006) 135–145.
[39] Q. Feng, Q. Lin, F. Gong, S. Sugita, M. Shoya, Adsorption of lead and mercury by rice husk ash, J. Colloid Interface Sci. 278 (1) (2004) 1–8.
[40] A. Sanchez, A. Ballester, L.M. Blazques, F. Gonzalez, J. Munoz, A. Hammaini, Biosorption of copper and zinc by *Cymodocea nodosa*, FEMS Microbiol. Rev. 23 (1999) 527–536.
[41] P. Kaewsarn, Biosorption of copper(II) from aqueous solution by pretreated biomass of marine algae *Padina* sp., Chemosphere 47 (2002) 1081–1085.
[42] A. Üçer, A. Uyanik, Ş.F. Aygün, Adsorption of Cu(II), Cd(II), Zn(II), Mn(II) and Fe(III) ions by tannic acid immobilized activated carbon, Sep. Purif. Technol. 47 (3) (2006) 113–118.
[43] J.P. Chen, S. Wu, K.H. Chong, Surface modification of a granular activated carbon by citric acid for enhancement of copper adsorption, Carbon 41 (10) (2003) 1979–1986.
[44] E. Álvarez-Ayuso, A. García-Sánchez, Sepiolite as a feasible soil additive for the immobilization of cadmium and zinc, Sci. Total Environ. 305 (1–3) (2003) 1–12.
[45] M. Sprynskyy, B.B. Artur, P. Terzyk, J. Namieśnik, Study of the selection mechanism of heavy metal (Pb^{2+}, Cu^{2+}, Ni^{2+}, and Cd^{2+}) adsorption on clinoptilolite, J. Colloid Interface Sci. 304 (1) (2006) 21–28.